Geometric frustration in the class of exactly solvable Ising–Heisenberg diamond chains

2006 J. Phys.: Condens. Matter 18 4967

(http://iopscience.iop.org/0953-8984/18/20/020)

INSTITUTE OF PHYSICS PUBLISHING JOURNAL OF PHYSICS: CONDENSED MATTER

J. Phys.: Condens. Matter **18** (2006) 4967–4984 doi:10.1088/0953-8984/18/20/020

Geometric frustration in the class of exactly solvable Ising–Heisenberg diamond chains

Lucia Čanová, Jozef Strečka[1] **and Michal Jaščur**

Department of Theoretical Physics and Astrophysics, Faculty of Science, P J Šafárik University, Park Angelinum 9, 040 01 Košice, Slovak Republic

E-mail: lucia.canova@post.sk and jozkos@pobox.sk

Received 13 March 2006
Published 5 May 2006
Online at stacks.iop.org/JPhysCM/18/4967

Abstract

Ground-state and finite-temperature properties of the mixed spin-$\frac{1}{2}$ and spin-S Ising–Heisenberg diamond chains are examined within an exact analytical approach based on the generalized decoration–iteration map. A particular emphasis is laid on the investigation of the effect of geometric frustration, which is generated by the competition between Heisenberg- and Ising-type exchange interactions. It is found that an interplay between the geometric frustration and quantum effects gives rise to several quantum ground states with entangled spin states in addition to some semi-classically ordered ones. Among the most interesting results to emerge from our study one could mention rigorous evidence for quantized plateaux in magnetization curves, an appearance of the round minimum in the thermal dependence of susceptibility times temperature data, double-peak zero-field specific heat curves, or an enhanced magnetocaloric effect when the frustration comes into play. The triple-peak specific heat curve is also detected when applying small external field to the system driven by the frustration into the disordered state.

1. Introduction

Over the last three decades, the low-dimensional quantum spin models with competing (frustrated) interactions have attracted considerable research interest, especially due to their extraordinary diverse ground-state behaviour. *Geometrically frustrated spin systems* constitute a special sub-class of the frustrated models that can be distinguished by incapability of spins, inherent in their lattice positions, to simultaneously minimize the ground-state energy of each individual spin–spin interaction [1]. As a rule, the quantum spin systems affected by a rather strong geometric frustration often exhibit an exotic non-magnetic ground state (which does not have its classical analogue) in addition to a rich variety of the semi-classically ordered ones [2].

[1] Author to whom any correspondence should be addressed.

It is worthy of notice, moreover, that a subtle interplay between the geometric frustration and quantum fluctuations gives rise to a number of intriguing phenomena including the macroscopic degeneracy of ground state [3], order by disorder effect [4], chirality [5], quantum phase transitions [6–8], quantized plateaux in the magnetization curves [8–10], double-peak specific heat curves [11–13], enhanced magnetocaloric effect [14–17], etc.

Despite a significant amount of effort, there are only a few frustrated spin-$\frac{1}{2}$ quantum Heisenberg models, such as the Majumdar–Ghosh model on the double chain [18–21], the sawtooth (Δ) chain [22–25], or the Shastry–Sutherland model [26], for which precise analytic solution is available at least for the ground state. Nevertheless, it should be pointed out that frustrated quantum systems are in general rather difficult to deal with, since extensive numerical methods must be used in order to obtain a reliable estimate of their magnetic properties. From this point of view, the one-dimensional (1D) frustrated spin systems are the simplest systems with respect to accurate treatment. Of these systems, the spin-$\frac{1}{2}$ quantum Heisenberg model with *diamond chain* topology is currently actively engaged in the investigation of geometric frustration. Interestingly, this simple quantum system turned out to have rather complex ground state; apart from the usual ferrimagnetic phase there are in fact several quantum dimerized and plaquette states involved in the zero-field ground-state phase diagram [27–29]. Further studies devoted to the spin-$\frac{1}{2}$ quantum Heisenberg model on the diamond chain have provided fairly accurate results for the ground-state phase diagram in a presence of the external field [30–32], the spin gap [33], the magnetization and the susceptibility [34]. Another remarkable finding relates to the observation of an inversion phenomenon, which can be induced in the frustrated diamond chain through the exchange anisotropy [35, 36]. Note that the ground state and thermodynamics of the mixed-spin diamond chains also containing higher-spin sites have already been particularly examined as well [37–41].

It is worthwhile to remark that 1D frustrated spin systems have initially been introduced purely as toy models suitable for investigating the effect of spin frustration. However, recent progress achieved in the design and controlled synthesis of molecular-based magnetic materials afforded another stimulus for testing 1D frustrated spin systems by overcoming the lack of desirable model compounds. As a matter of fact, the rapidly expanding field of molecular engineering has led to fabrication of several coordination polymers, which can be regarded as genuine examples of the frustrated spin models [42]. With the help of structural data known long ago [43], Kikuchi and co-workers [44–52] have recognized $Cu_3(CO_3)_2(OH)_2$ (azurite) as an appropriate candidate for the diamond chain compound. Experimental data measured for the high-field magnetization, susceptibility, specific heat, NMR [44–47] and ESR data [48–52] have indeed confirmed Kikuchi's conjecture and it is now quite well established that the azurite represents the actual material for the frustrated diamond chain. It should also be mentioned that sufficiently strong frustration found in the azurite clearly manifests itself in its quantum features: the high-field magnetization shows a quantum plateau at one-third of the saturation magnetization, the susceptibility turned out to have two round peaks at relatively low temperatures and ESR data have proven the gapless excitation spectrum. Theoretical interest focused on the diamond chain structure also enhances its other experimental realizations provided by the polymeric compounds such as Cu_2OSO_4 [53] and $M_3(OH)_2$ (M = Ni, Co, Mn) [54–57].

With this background, we shall investigate in the present article a simplified version of the frustrated Ising–Heisenberg diamond chain, which can exactly be solved by applying an accurate map based on the generalized decoration–iteration transformation [58, 59]. It is noteworthy that this relatively simple and straightforward analytical approach has recently been adapted to study an appearance of quantized plateaux in the magnetization process of the trimerized [60, 61] and tetramerized [62, 63] Ising–Heisenberg linear chains. As we shall

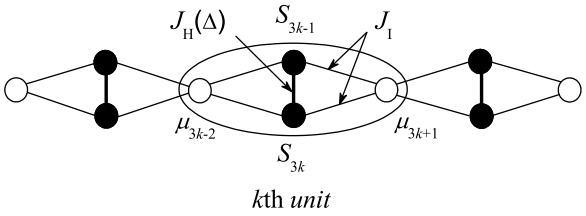

Figure 1. Diagrammatic representation of the mixed-spin Ising–Heisenberg diamond chain. The empty (filled) circles denote the lattice positions of the Ising (Heisenberg) spins; the ellipse demarcates kth diamond-shaped plaquette.

show hereafter, the same strategy can also be used to explore the frustrated Ising–Heisenberg diamond chain, which represents another particular realization of models tractable within the generalized algebraic maps. The main goal of the present work is to exploit a grand advance of the method used for obtaining exact results for all possible ground states as well as all basic thermodynamic quantities.

The rest of this paper is organized as follows. The model Hamiltonian and major features of the mapping method are presented in section 2. Section 3 is divided into two subsections. In the former one, we provide rigorous results for the spin-$\frac{1}{2}$ Ising–Heisenberg diamond chain, while the latter one comprises magnetic data of the mixed spin-$\frac{1}{2}$ and spin-1 Ising–Heisenberg diamond chain. Altogether, exact results for ground-state phase diagrams, magnetization, entropy, susceptibility and specific heat are derived and particularly discussed for both investigated diamond chains. A cooling rate of adiabatic demagnetization is also explored in connection with the enhanced magnetocaloric effect. Finally, some concluding remarks are drawn in section 4.

2. The model and its exact solution

Let us begin by considering two kinds of spins regularly distributed on the 1D lattice composed of the diamond-shaped units as diagrammatically depicted in figure 1. To ensure an exact tractability of this spin system, we shall further suppose that each diamond-shaped plaquette consists of two dumbbell *Heisenberg* spins (S), which are placed in between two *Ising* spins (μ) residing in corner-sharing positions on the diamond motifs. For further convenience, we shall write the total Hamiltonian as a sum over plaquette Hamiltonians, i.e. $\hat{\mathcal{H}} = \sum_{k=1}^{N} \hat{\mathcal{H}}_k$, where each plaquette Hamiltonian $\hat{\mathcal{H}}_k$ involves all interaction terms associated with one diamond-shaped unit (see figure 1)

$$\hat{\mathcal{H}}_k = J_H[\Delta(\hat{S}^x_{3k-1}\hat{S}^x_{3k} + \hat{S}^y_{3k-1}\hat{S}^y_{3k}) + \hat{S}^z_{3k-1}\hat{S}^z_{3k}] + J_I(\hat{S}^z_{3k-1} + \hat{S}^z_{3k})(\hat{\mu}^z_{3k-2} + \hat{\mu}^z_{3k+1}) - H_H(\hat{S}^z_{3k-1} + \hat{S}^z_{3k}) - H_I(\hat{\mu}^z_{3k-2} + \hat{\mu}^z_{3k+1})/2. \quad (1)$$

Above, $\hat{\mu}^z_k$ and $\hat{S}^\alpha_k$ ($\alpha = x, y, z$) denote spatial components of the spin-$\frac{1}{2}$ and spin-S operators, the parameter J_H stands for the anisotropic XXZ interaction between the nearest-neighbouring Heisenberg (dumbbell) spins and the parameter J_I accounts for the Ising-type coupling between the Heisenberg spins and their nearest Ising neighbours. The parameter Δ allows us to control the Heisenberg exchange interaction J_H between the easy-axis ($\Delta < 1$) and easy-plane ($\Delta > 1$) regime and finally, the last two terms incorporate coupling of the Ising and Heisenberg spins to an external longitudinal magnetic field H_I and H_H, respectively.

The crucial point of our calculation represents calculation of the partition function. By making use of the commutation rule between different plaquette Hamiltonians, i.e. by

exploiting $[\hat{\mathcal{H}}_k, \hat{\mathcal{H}}_l] = 0$ valid for each $k \neq l$, the partition function of the Ising–Heisenberg diamond chain can be partially factorized into the following product:

$$\mathcal{Z} = \sum_{\{\mu_i\}} \prod_{k=1}^{N} \mathrm{Tr}_k \exp(-\beta \hat{\mathcal{H}}_k), \tag{2}$$

where $\beta = 1/(k_{\mathrm{B}}T)$, k_{B} is Boltzmann's constant, T the absolute temperature, the symbol $\sum_{\{\mu_i\}}$ means a summation over all available configurations of Ising spins $\{\mu_i\}$ and Tr_k stands for a trace over spin degrees of freedom of two dumbbell Heisenberg spins belonging to the kth diamond unit. After performing this partial trace, the structure of relation (2) immediately implies a possibility of applying the generalized decoration–iteration mapping transformation [58, 59]

$$\begin{aligned}\mathrm{Tr}_k \exp(-\beta \hat{\mathcal{H}}_k) &= \exp\big[\beta H_{\mathrm{I}}(\mu^z_{3k-2} + \mu^z_{3k+1})/2\big] G\big[\beta J_{\mathrm{I}}(\mu^z_{3k-2} + \mu^z_{3k+1})\big] \\ &= A \exp\big[\beta R \mu^z_{3k-2}\mu^z_{3k+1} + \beta H_0(\mu^z_{3k-2} + \mu^z_{3k+1})/2\big],\end{aligned} \tag{3}$$

which converts the Ising–Heisenberg diamond chain into the uniform spin-$\frac{1}{2}$ Ising linear chain with an effective nearest-neighbour coupling R and an effective external field H_0. The expression $G(x)$ in the first line of equation (3) depends on the spin of the Heisenberg atoms and its explicit form is given in the appendix for two particular spin cases $S = \frac{1}{2}$ and 1. It is noteworthy that a general validity of the mapping relation (3) necessitates a self-consistency condition to be satisfied, which means that it must hold independently of spin states of both Ising spins μ_{3k-2} and μ_{3k+1}. It can readily be proved that a substitution of four possible configurations of the Ising spins μ_{3k-2} and μ_{3k+1} into the formula (3) indeed gives just three independent equations, which unambiguously determine the unknown mapping parameters A, R and H_0,

$$A = \big(G_1 G_2 G_3^2\big)^{1/4}, \qquad \beta R = \ln\left(\frac{G_1 G_2}{G_3^2}\right), \qquad \beta H_0 = \beta H_{\mathrm{I}} + \ln\left(\frac{G_1}{G_2}\right). \tag{4}$$

Here, we have defined the functions $G_1 = G(\beta J_{\mathrm{I}})$, $G_2 = G(-\beta J_{\mathrm{I}})$ and $G_3 = G(0)$ in order to write the transformation parameters A, R and H_0 in more abbreviated and general form. Now, a direct substitution of the transformation (3) into the expression (2) yields the equality

$$\mathcal{Z}(\beta, J_{\mathrm{I}}, J_{\mathrm{H}}, \Delta, H_{\mathrm{I}}, H_{\mathrm{H}}) = A^N \mathcal{Z}_0(\beta, R, H_0), \tag{5}$$

which establishes an exact mapping relationship between the partition function $\mathcal{Z}$ of the Ising–Heisenberg diamond chain and, respectively, the partition function $\mathcal{Z}_0$ of the uniform spin-$\frac{1}{2}$ Ising linear chain defined by means of the nearest-neighbour coupling R and the effective field H_0. Notice that the exact solution for the partition function of the latter system is well known (see for instance [64]) and hence the relation (5) can readily be utilized for calculation of some important quantities (magnetization, entropy, specific heat and susceptibility) by making use of the standard thermodynamical–statistical relations. It should be mentioned, however, that there also exists another alternative approach that is of particular importance if some relevant physical quantity cannot be obtained within this procedure. Actually, the problem connected with the calculation of correlation functions and/or quadrupolar moment can be simply avoided by employing the following exact spin identities:

$$\langle f_1(\hat{\mu}^z_1, \ldots, \hat{\mu}^z_{3k-2}, \ldots, \hat{\mu}^z_{3N-2})\rangle = \langle f_1(\hat{\mu}^z_1, \ldots, \hat{\mu}^z_{3k-2}, \ldots, \hat{\mu}^z_{3N-2})\rangle_0, \tag{6}$$

$$\langle f_2(\hat{\mu}^z_{3k-2}, \hat{S}^{\alpha}_{3k-1}, \hat{S}^{\gamma}_{3k}, \hat{\mu}^z_{3k+1})\rangle = \left\langle \frac{\mathrm{Tr}_k\, f_2(\hat{\mu}^z_{3k-2}, \hat{S}^{\alpha}_{3k-1}, \hat{S}^{\gamma}_{3k}, \hat{\mu}^z_{3k+1}) \exp(-\beta \hat{\mathcal{H}}_k)}{\mathrm{Tr}_k \exp(-\beta \hat{\mathcal{H}}_k)} \right\rangle. \tag{7}$$

In the above, the function f_1 depends exclusively on the Ising spin variables $\{\mu_i\}$, while the function f_2 may depend on any spin variable belonging to the kth diamond plaquette. The

superscripts $\alpha, \gamma \in (x, y, z)$ label spatial components of the appropriate spin operators, and finally the symbols $\langle \cdots \rangle$ and $\langle \cdots \rangle_0$ stand for the standard canonical average performed over the ensemble defined on the Ising–Heisenberg diamond chain and its corresponding Ising chain, respectively. By applying the exact spin identities (6) and (7), one easily attains rigorous results for the sub-lattice magnetization m_{i}^z and m_{h}^z reduced per Ising and Heisenberg spin, respectively, and the pair correlation functions c_{hh}^{xx}, c_{hh}^{zz} and c_{ih}^{zz}, as well as the quadrupolar moment q_{hh}^{zz}

$$m_{\mathrm{i}}^z \equiv \langle \hat{\mu}_{3k-2}^z \rangle = \langle \hat{\mu}_{3k-2}^z \rangle_0 \equiv m_0, \tag{8}$$

$$c_{\mathrm{ii}}^z \equiv \langle \hat{\mu}_{3k-2}^z \hat{\mu}_{3k+1}^z \rangle = \langle \hat{\mu}_{3k-2}^z \hat{\mu}_{3k+1}^z \rangle_0 \equiv \varepsilon_0, \tag{9}$$

$$m_{\mathrm{h}}^z \equiv \langle \hat{S}_{3k}^z \rangle = K_1/4 + m_0 L_1 + \varepsilon_0 M_1, \tag{10}$$

$$c_{\mathrm{hh}}^{zz} \equiv \langle \hat{S}_{3k-1}^z \hat{S}_{3k}^z \rangle = K_2/4 + m_0 L_2 + \varepsilon_0 M_2, \tag{11}$$

$$c_{\mathrm{hh}}^{xx} \equiv \langle \hat{S}_{3k-1}^x \hat{S}_{3k}^x \rangle = K_3/4 + m_0 L_3 + \varepsilon_0 M_3, \tag{12}$$

$$c_{\mathrm{ih}}^{zz} \equiv \langle \hat{\mu}_{3k-2}^z \hat{S}_{3k-1}^z \rangle = L_1/8 + m_0(K_1 + M_1)/4 + \varepsilon_0 L_1/2, \tag{13}$$

$$q_{\mathrm{hh}}^{zz} \equiv \langle (\hat{S}_{3k-1}^z)^2 \rangle = K_4/4 + m_0 L_4 + \varepsilon_0 M_4. \tag{14}$$

As one can see, all afore-listed quantities can be expressed in terms of the single-site magnetization m_0 and the nearest-neighbour correlation ε_0 of the spin-$\frac{1}{2}$ Ising linear chain given by R and H_0. Since exact analytical formulae for those quantities have been obtained in the literature many times before [64], we shall restrict ourselves for brevity to listing the coefficients K_i, L_i and M_i ($i = 1$–4) emerging in the set of equations (8)–(14)

$$K_i = F_i(\beta J_{\mathrm{I}}) + F_i(-\beta J_{\mathrm{I}}) + 2F_i(0), \tag{15}$$

$$L_i = F_i(\beta J_{\mathrm{I}}) - F_i(-\beta J_{\mathrm{I}}), \tag{16}$$

$$M_i = F_i(\beta J_{\mathrm{I}}) + F_i(-\beta J_{\mathrm{I}}) - 2F_i(0). \tag{17}$$

An explicit representation of the functions $F_i(x)$ is too cumbersome to write it down here and it is therefore left for the appendix.

Finally, we simply quote the well known thermodynamical–statistical relations, which have been utilized for calculating Gibbs free energy $\mathcal{G}$, entropy S, specific heat C and susceptibility χ. Accurate results for these quantities have been obtained with the help of the precise mapping relation (5) and using

$$\mathcal{G} = -k_{\mathrm{B}} T \ln \mathcal{Z} = \mathcal{G}_0 - N k_{\mathrm{B}} T \ln A, \tag{18}$$

$$S = -\left(\frac{\partial \mathcal{G}}{\partial T}\right)_H, \qquad C = -T\left(\frac{\partial^2 \mathcal{G}}{\partial T^2}\right)_H, \qquad \chi = -\left(\frac{\partial^2 \mathcal{G}}{\partial H^2}\right)_T, \tag{19}$$

where $\mathcal{G}_0$ is referred to as the Gibbs free energy of corresponding spin-$\frac{1}{2}$ Ising chain [64].

3. Results and discussion

Before proceeding to a discussion of the most interesting results it is worth mentioning that the results derived in the preceding section hold regardless of whether ferromagnetic or antiferromagnetic interactions are assumed. As we are mainly interested in examination of the spin frustration effect, in what follows we restrict both exchange parameters J_{H} and J_{I} to positive values in order to match the situation in the frustrated antiferromagnetic diamond chain. Furthermore, it is convenient to reduce the number of free parameters by assuming equal g-factors for the Ising and Heisenberg spins, i.e. by imposing the same parameter representing the effect of external field $H_{\mathrm{I}} = H_{\mathrm{H}} = H$. To simplify further discussion, we shall also introduce a set of reduced parameters $t = k_{\mathrm{B}}T/J_{\mathrm{I}}$, $h = H/J_{\mathrm{I}}$ and $\alpha = J_{\mathrm{H}}/J_{\mathrm{I}}$ as describing dimensionless temperature, external field and the strength of frustration, respectively.

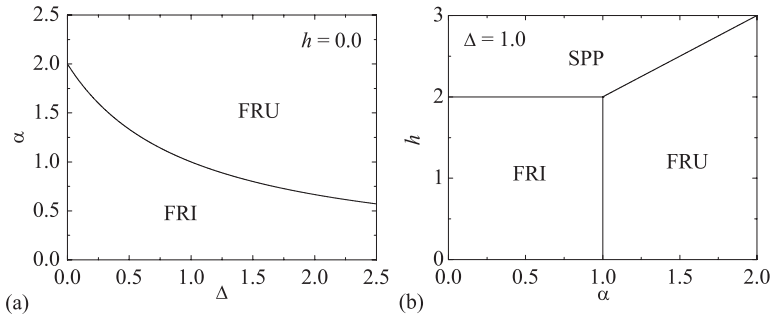

Figure 2. (a) Ground-state phase diagram in the Δ–α plane for the system in the absence of an external magnetic field; (b) ground-state phase diagram in the α–h plane for $\Delta = 1.0$. Spin order $|\mathrm{FRI}\rangle$, $|\mathrm{FRU}\rangle$ and $|\mathrm{SPP}\rangle$ to emerge within different sectors of phase diagrams is unambiguously determined by the wavefunctions (20)–(22), respectively.

3.1. Spin-$\frac{1}{2}$ Ising–Heisenberg diamond chain

First, let us take a closer look at the ground state of the spin-$\frac{1}{2}$ Ising–Heisenberg diamond chain. For illustration, two ground-state phase diagrams are displayed in figure 2, one in the Δ–α space for the system without external magnetic field (figure 2(a)) and the other one in the α–h space for the system placed in the non-zero external field under the assumption $\Delta = 1.0$ (figure 2(b)). Both the figures clearly demonstrate that a competition between the interaction parameters α, Δ and h gives rise to three possible ground states. Apart from the usual ferrimagnetic phase (FRI) and the frustrated phase (FRU) found both in the presence as well as the absence of the external field, the system ends up in the saturated paramagnetic phase (SPP) once the external field is stronger than its saturation value. Spin orders within FRI, FRU and SPP can be distinguished from one another according to their attributes (physical quantities included in the set of equations (8)–(14)), as well as through their wavefunctions

$$|\mathrm{FRI}\rangle = \prod_{k=1}^{N} |-\rangle_{3k-2} \prod_{k=1}^{N} |+,+\rangle_{3k-1,3k},$$
$$m_{\mathrm{i}}^{z} = -0.5,\ m_{\mathrm{h}}^{z} = 0.5,\ c_{\mathrm{hh}}^{zz} = 0.25,\ c_{\mathrm{hh}}^{xx} = 0,\ c_{\mathrm{ih}}^{zz} = -0.25; \tag{20}$$

$$|\mathrm{FRU}\rangle = \prod_{k=1}^{N} |\pm\rangle_{3k-2} \prod_{k=1}^{N} \frac{1}{\sqrt{2}}(|+,-\rangle - |-,+\rangle)_{3k-1,3k},$$
$$m_{\mathrm{i}}^{z} = 0,\ m_{\mathrm{h}}^{z} = 0,\ c_{\mathrm{hh}}^{zz} = -0.25,\ c_{\mathrm{hh}}^{xx} = -0.25,\ c_{\mathrm{ih}}^{zz} = 0; \tag{21}$$

$$|\mathrm{SPP}\rangle = \prod_{k=1}^{N} |+\rangle_{3k-2} \prod_{k=1}^{N} |+,+\rangle_{3k-1,\,3k},$$
$$m_{\mathrm{i}}^{z} = 0.5,\ m_{\mathrm{h}}^{z} = 0.5,\ q_{\mathrm{hh}}^{zz} = 0.25,\ c_{\mathrm{hh}}^{zz} = 0.25,\ c_{\mathrm{hh}}^{xx} = 0,\ c_{\mathrm{ih}}^{zz} = 0.25. \tag{22}$$

The first product in the afore-listed eigenfunctions is carried out over all Ising spins, the second one runs over all pairs of the Heisenberg dumbbell spins and $|\pm\rangle$ denotes the standard ket vector assigned to the zth projection of the Ising ($\mu^z = \pm\frac{1}{2}$) and Heisenberg ($S^z = \pm\frac{1}{2}$) spins. It is quite evident from the set of equations (20) that FRI displays the classical ferrimagnetic spin arrangement usually observed in the pure Ising systems; actually, all the results clearly indicate antiparallel alignment between the nearest-neighbouring Ising and Heisenberg spins. It should be emphasized, however, that the classical ferrimagnetic order originating from the antiferromagnetic Ising interaction J_{I} can be destroyed through the competing Heisenberg

interaction $J_{\mathrm{H}}(\Delta)$ that brings a frustration into play. As a matter of fact, the spin order dramatically changes when the frustration parameter α exceeds the boundary value

$$|\mathrm{FRI}\rangle - |\mathrm{FRU}\rangle : \alpha_{\mathrm{b}} = \frac{2}{\Delta + 1}. \tag{23}$$

In such a case, all Heisenberg spin pairs create singlet dimers, and on account of this singlet pairing all Ising spins become completely free to flip. In other words, the Ising spins are thoroughly uncorrelated in FRU due to their frustration arising from the singlet pairing between the Heisenberg spins as also suggested by (21). Owing to this fact, it might be concluded that the diamond spin chain splits into a set of independent monomers (Ising spins) and dimers (Heisenberg spin pairs) whenever the frustration parameter is stronger than its boundary value α_{b}. Thus, FRU virtually represents a macroscopically degenerate monomer–dimer state with the residual entropy $S_{\mathrm{res}}/3N = \ln(2)^{1/3}$ proportional to the total number of frustrated Ising spins. For completeness, it should be also noticed that sufficiently strong external field stabilizes the standard SPP regardless whether FRI or FRU constitutes the zero-field ground state (see figure 2(b)). As could be expected, all Ising as well as Heisenberg spins tend to align into the external-field direction above the saturation field, which represents the lower bound for an occurrence of SPP.

At this stage, it is worthwhile to compare our results with those obtained by Takano, Kubo and Sakamoto for the spin-$\frac{1}{2}$ Heisenberg model on the diamond chain [27]. It is noteworthy that the zero-field ground state of the full Heisenberg model constitutes the ferrimagnetic phase, tetramer–dimer and dimer–monomer phases depending on whether $\alpha < 0.909$, $0.909 < \alpha < 2.0$, or $\alpha > 2.0$, respectively. In this regard, the ferrimagnetic and monomer–dimer phases are separated by means of the tetramer–dimer phase, and as a consequence of this a direct frustration-induced transition does not occur between them. Apparently, the Ising–Heisenberg model under investigation cannot render the intermediate tetramer–dimer phase, since the Ising spins located at the corner-sharing positions of each diamond motif represent a barrier for the quantum fluctuations and thus they cannot form tetramers with the Heisenberg spin pairs creating triplets, as in the case of the diamond chain described by the isotropic Heisenberg Hamiltonian. In spite of this qualitative rather than quantitative difference, it is interesting to confront our result for the FRI–FRU boundary $\alpha_{\mathrm{b}} = 1.0$ (for $\Delta = 1.0$) with the $\alpha = 0.909$ reported for the boundary between the ferrimagnetic and tetramer–dimer phase. Namely, both the boundaries reflect a transition from the ferrimagnetic state with the non-zero total magnetization to a disordered state (either tetramer–dimer or dimer–monomer) where the frustration leads to zero total magnetization.

Next, we turn our attention to the magnetization process at zero as well as non-zero temperatures. For this purpose, two typical magnetization versus field dependences are plotted in figure 3 for several dimensionless temperatures. It can be readily understood by comparing the displayed magnetization curves with the phase diagram shown in figure 2(b) that two different zero-temperature limits obviously reflect both possible types of field-induced transitions, FRI–SPP (figure 3(a)) and FRU–SPP (figure 3(b)). Since the ground state is being formed in the former (latter) case by FRI (FRU), the zero-temperature magnetization curve depicted in figure 3(a) (figure 3(b)) starts from non-zero (zero) magnetization in the limit of vanishing external field. In contrast to this, both magnetization curves always start from zero magnetization (disordered state) at any finite temperature according to the one-dimensional character of the investigated spin system. It should be emphasized, moreover, that the magnetization jumps to be observed in the magnetization curves strictly at $t = 0$ are gradually smeared out when temperature is raised from zero. In addition, the higher the temperature, the smaller the width of magnetization plateaux (horizontal regions in the magnetization versus field dependence), which entirely disappear from the magnetization curves above a certain

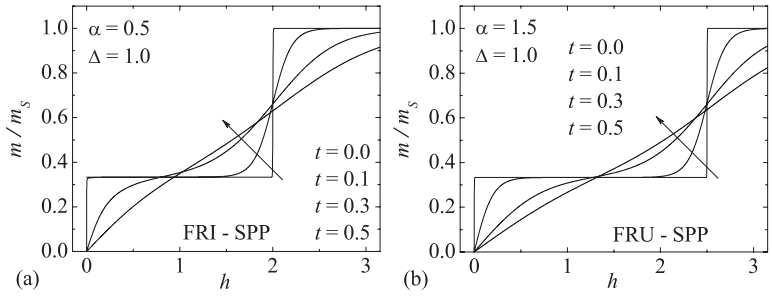

Figure 3. The total magnetization reduced with respect to its saturation value versus the external magnetic field at various temperatures $t = 0.0, 0.1, 0.3, 0.5$ in ascending order along the direction of arrows.

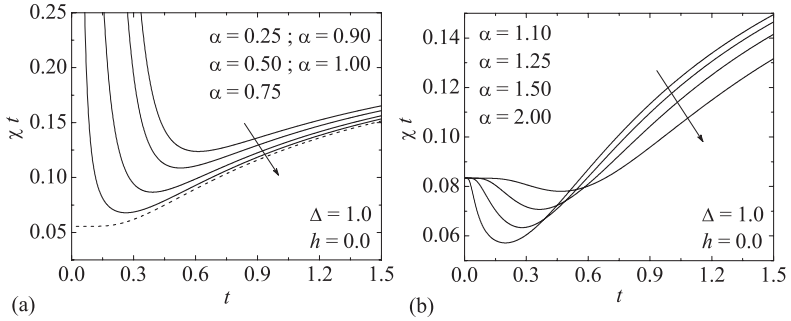

Figure 4. Thermal dependence of the zero-field susceptibility times temperature data for $\Delta = 1.0$, $\alpha = 0.25, 0.5, 0.75, 0.9, 1.0$ (a) and $\Delta = 1.0$, $\alpha = 1.1, 1.25, 1.5, 2.0$ (b) in ascending order along the direction of arrows. For clarity, the case $\alpha_c = 1.0$ corresponding to the FRI–FRU phase boundary is depicted as a broken line.

temperature. Finally, it is quite interesting to mention that the identified magnetization plateaux at one third of the saturation magnetization satisfy the Oshikawa–Yamanaka–Affleck rule [67] proposed for the formation of quantized plateaux.

Now, let us step forward to a discussion concerned with the thermal dependence of the zero-field susceptibility times temperature (χt) data as displayed in figure 4. If the frustration parameter α is selected so that FRI constitutes the ground state (figure 4(a)), then χt data exhibit a round minimum prior to exponential divergence appearing on temperature decrease. As can be clearly seen from figure 4(a), the stronger the frustration parameter α, the deeper the notable minimum whose position is simultaneously shifted towards lower temperatures. It should be mentioned, moreover, that the appearance of a round minimum in the t–χt dependence is a typical feature of quantum ferrimagnets, since the χt product monotonically decreases with temperature for ferromagnets, while it monotonically increases for antiferromagnets [68–71]. Accordingly, the location of the round minimum can be regarded as a point that determines ferromagnetic-to-antiferromagnetic crossover in view of thermal excitations. On the other hand, if the frustration parameter α drives the system into the disordered FRU ground state (figure 4(b)), the χt product then exhibits a round minimum before it tends to the constant value $1/12$ by approaching zero temperature. Notice that this zero-temperature value can be explained in compliance with the Curie law of the frustrated Ising spins, which effectively form isolated spins (monomers) in FRU.

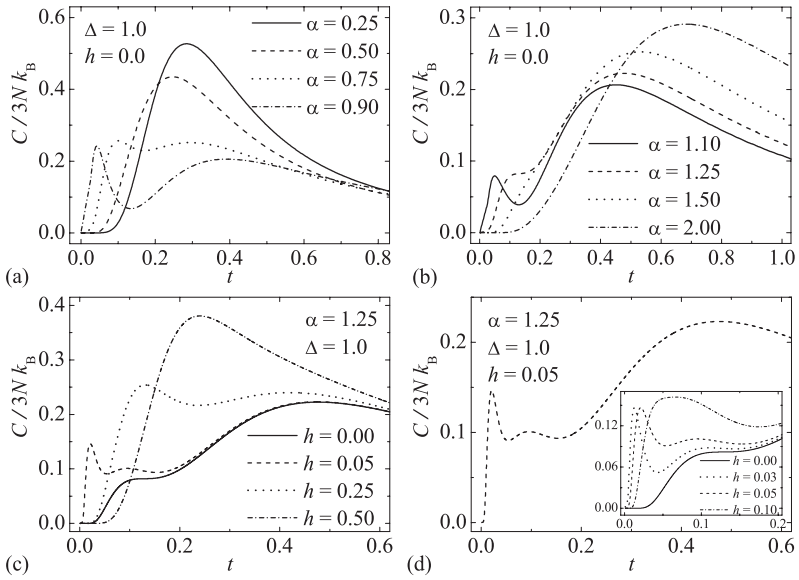

Figure 5. Temperature variations of the specific heat when $\Delta = 1.0$ is fixed. ((a), (b)) illustrate the effect of frustration parameter α on the shape of zero-field specific heat and ((c), (d)) display the effect of the applied external magnetic field when the frustration parameter $\alpha = 1.25$ drives the system into the disordered FRU state.

Another quantity, which is important for overall understanding of thermodynamics, represents the specific heat. Temperature variations of the zero-field specific heat are depicted in figures 5(a) and (b) for $\Delta = 1.0$ and several values of the frustration parameter α. According to these plots, there still emerges at least one round maximum, which can be thought of as the usual Schottky-type maximum, irrespective of whether FRI or FRU constitutes the ground state. If the frustration parameter is selected sufficiently close to the FRI–FRU phase boundary given by α_b, however, there also appears an additional second maximum located in the low-temperature part of the specific heat. Apparently, the low-temperature peak becomes more pronounced, the closer α is selected to α_b. When the frustration parameter α drives the system into the disordered FRU ground state, then the striking second maximum gradually disappears upon further strengthening of α, since the low-temperature peak shifts towards higher temperatures until it entirely merges with the high-temperature Schottky-type maximum (see the curves labelled as $\alpha = 1.1$, 1.25 and 1.5). These observations would suggest that the double-peak structure in the specific heat curves originates from thermal excitations between the ground-state spin configuration and the ones close enough in energy to the ground state.

The situation becomes even more intriguing on applying the external magnetic field. As one can see from figure 5(c), the rising external field generally causes a gradual increase in the height of the low-temperature peak and moves it towards the higher temperatures. A similar trend is also seen in a change of the size and position of the high-temperature maximum, although this Schottky-like peak moves towards higher temperature more slowly than the low-temperature one. As a result, both maxima coalesce at a certain value of the external field, and above this value the specific heat exhibits just single rounded maximum (see for instance the curve $h = 0.5$). Apart from these rather trivial findings, a remarkable triple-peak specific heat curve can also be detected when small but non-zero external field is applied to the system driven by the frustration into the disordered FRU state (the case $h = 0.05$ in figure 5(c)).

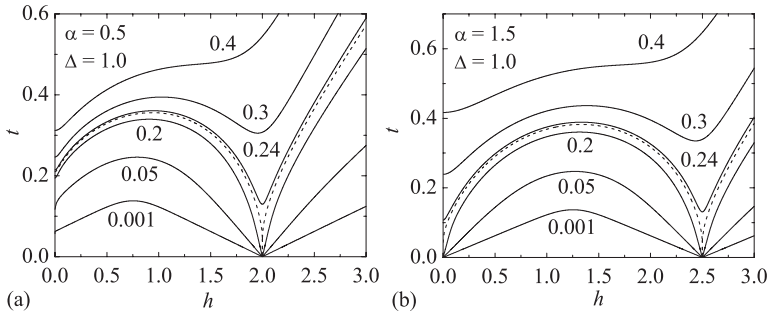

Figure 6. Adiabatic demagnetization in the form of temperature versus external field dependence for $\Delta = 1.0, \alpha = 0.5$ (a) and $\Delta = 1.0, \alpha = 1.5$ (b). For better orientation, the broken curve depicts the dependence when entropy is fixed at the residual value $S_{\rm res}/3N = \ln(2)^{1/3}$ of FRU.

Besides two afore-described peaks, whose origin has been resolved earlier, there also appears an additional third peak to be located at the lowest temperature. There are strong indications that an appearance of this additional sharp maximum can be explained through the field-induced splitting of the energy levels related to the frustrated Ising spins. In accordance with this statement, the inset of figure 5(d) clearly demonstrates how this peculiar third maximum gradually shifts towards higher temperatures with increasing field strength until it coalesces with the second low-temperature peak (see the curve labelled $h = 0.1$).

At last, we shall briefly discuss the adiabatic demagnetization curves studied in connection with the enhanced magnetocaloric effect. Some interesting results for adiabatic processes keeping entropy constant are presented in figure 6 in the form of the temperature versus external field dependence. Two depicted sets of demagnetization curves reflect two available adiabatic scenarios related to SPP $\rightarrow$ FRI (figure 6(a)) and SPP $\rightarrow$ FRU (figure 6(b)) transitions. Apparently, the maximal cooling rate emerges in the vicinity of critical fields and zero field, where zero temperature is in principle reached whenever the entropy is set equal to or less than its residual value $S_{\rm res}$. It should be pointed out that a relatively fast heating, which occurs when the external field is lowered from its critical value, prevents a practical use of the whole demagnetization curves for a cooling purpose. In addition, the cooling effect becomes of technological relevance only if the cooling rate exceeds the one of paramagnetic salts. From this point of view, the enhanced magnetocaloric effect is observed only if the frustration drives the system into the disordered FRU ground state (figure 6(b)). Even under this condition, the cooling rate of paramagnetic materials is exceeded only if the entropy is chosen close enough to its residual value $S_{\rm res}$ and the external field is below $h \approx 0.05$. This limitation would imply that temperatures in the sub-Kelvin range are in principle accessible provided that a frustrated diamond chain compound with exchange constants of the order of a few tenths of Kelvin, such as azurite, is used as refrigerant.

3.2. Mixed spin-$\frac{1}{2}$ and spin-1 Ising–Heisenberg diamond chain

In this part, we shall turn our attention to the mixed spin-$\frac{1}{2}$ and spin-1 Ising–Heisenberg diamond chain with the aim to clarify the impact of integer-valued Heisenberg spins on the magnetic behaviour of the frustrated diamond chain. We start our discussion repeatedly with the ground-state analysis. The phase diagram constructed in the absence of the external field (figure 7(a)) implies the existence of three possible ground states. Besides the semi-classically ordered ferrimagnetic phase (FRI), there also appear the quantum ferrimagnetic phase (QFI)

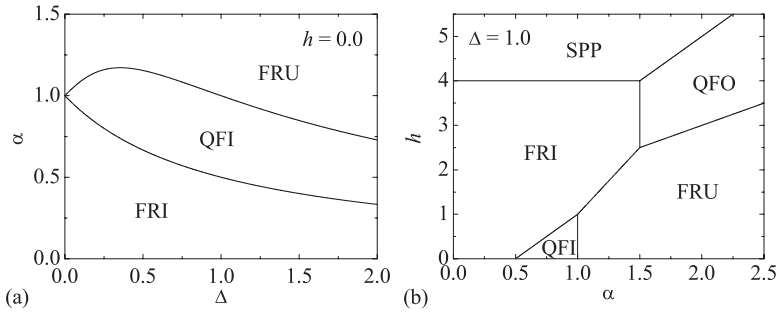

Figure 7. (a) Ground-state phase diagram in the absence of an external field; (b) ground-state phase diagram in the α–h plane for $\Delta = 1.0$. Spin order $|\mathrm{FRI}\rangle$, $|\mathrm{QFI}\rangle$, $|\mathrm{FRU}\rangle$, $|\mathrm{QFO}\rangle$ and $|\mathrm{SPP}\rangle$ emerging within different sectors of phase diagrams is unambiguously determined by the wavefunctions (24), (25), (26), (28) and (29), respectively.

and the frustrated phase (FRU). FRI, QFI and FRU can be characterized by means of

$$|\mathrm{FRI}\rangle = \prod_{k=1}^{N} |-\rangle_{3k-2} \prod_{k=1}^{N} |1,\,1\rangle_{3k-1,\,3k},$$
$$m_{\mathrm{i}}^{z} = -0.5,\, m_{\mathrm{h}}^{z} = 1,\, q_{\mathrm{hh}}^{zz} = 1,\, c_{\mathrm{hh}}^{zz} = 1,\, c_{\mathrm{hh}}^{xx} = 0,\, c_{\mathrm{ih}}^{zz} = -0.5; \tag{24}$$

$$|\mathrm{QFI}\rangle = \prod_{k=1}^{N} |-\rangle_{3k-2} \prod_{k=1}^{N} \frac{1}{\sqrt{2}}(|1,\,0\rangle - |0,\,1\rangle)_{3k-1,\,3k},$$
$$m_{\mathrm{i}}^{z} = -0.5,\, m_{\mathrm{h}}^{z} = 0.5,\, q_{\mathrm{hh}}^{zz} = 0.5,\, c_{\mathrm{hh}}^{zz} = 0,\, c_{\mathrm{hh}}^{xx} = -0.5,\, c_{\mathrm{ih}}^{zz} = -0.25; \tag{25}$$

$$|\mathrm{FRU}\rangle = \prod_{k=1}^{N} |\pm\rangle_{3k-2} \prod_{k=1}^{N} \frac{1}{2\sqrt{\delta}}\Big[\sqrt{\delta+1}(|1,-1\rangle + |-1,1\rangle) - \sqrt{2}\sqrt{\delta-1}|0,0\rangle\Big]_{3k-1,3k},$$
$$m_{\mathrm{i}}^{z} = 0,\, m_{\mathrm{h}}^{z} = 0,\, q_{\mathrm{hh}}^{zz} = -c_{\mathrm{hh}}^{zz} = (1+\delta^{-1})/2,\, c_{\mathrm{hh}}^{xx} = -2\Delta\delta^{-1},\, c_{\mathrm{ih}}^{zz} = 0; \tag{26}$$

where $\delta = \sqrt{1+8\Delta^2}$, the first product in the afore-listed eigenfunctions is taken over all Ising spins ($|\pm\rangle$ stands for $\mu^z = \pm\frac{1}{2}$) and the second product runs over all pairs of the Heisenberg dumbbell spins ($|\pm 1, 0\rangle$ is assigned to $S^z = \pm 1, 0$). Analytic expressions for the phase boundaries depicted in figure 7(a) read

$$|\mathrm{FRI}\rangle - |\mathrm{QFI}\rangle : \alpha_{\mathrm{b1}} = \frac{1}{\Delta+1}; \qquad |\mathrm{QFI}\rangle - |\mathrm{FRU}\rangle : \alpha_{\mathrm{b2}} = \frac{2\Delta - 1 + \delta}{2\Delta(\Delta+1)}. \tag{27}$$

The most significant difference between the two investigated diamond chains apparently rests in the presence of QFI located in between FRI and FRU. This observation would suggest that the geometric frustration initially favours a rise of QFI before it finally energetically stabilizes FRU. Accordingly, it might be concluded that a direct frustration-induced transition between FRI and FRU may not occur in the mixed spin-$\frac{1}{2}$ and spin-1 diamond chain except the one observable in the Ising limit ($\Delta = 0$).

Next, the ground-state phase diagram reflecting the effect of external field is shown in figure 7(b). This phase diagram suggests that in response to the applied external field there also may arise the quantum ferromagnetic phase (QFO) and the saturated paramagnetic phase (SPP) besides the aforementioned FRI, QFI and FRU phases

$$|\mathrm{QFO}\rangle = \prod_{k=1}^{N} |+\rangle_{3k-2} \prod_{k=1}^{N} \frac{1}{\sqrt{2}}(|1,\,0\rangle - |0,\,1\rangle)_{3k-1,3k},$$
$$m_{\mathrm{i}}^{z} = 0.5,\, m_{\mathrm{h}}^{z} = 0.5,\, q_{\mathrm{hh}}^{zz} = 0.5,\, c_{\mathrm{hh}}^{zz} = 0,\, c_{\mathrm{hh}}^{xx} = -0.5,\, c_{\mathrm{ih}}^{zz} = 0.25; \tag{28}$$

$$|\mathrm{SPP}\rangle = \prod_{k=1}^{N} |+\rangle_{3k-2} \prod_{k=1}^{N} |1,1\rangle_{3k-1,3k},$$
$$m_{\mathrm{i}}^{z} = 0.5, m_{\mathrm{h}}^{z} = 1, q_{\mathrm{hh}}^{zz} = 1, c_{\mathrm{hh}}^{zz} = 1, c_{\mathrm{hh}}^{xx} = 0, c_{\mathrm{ih}}^{zz} = 0.5. \quad (29)$$

Before proceeding further, let us make a few comments on all these possible ground states. Since FRI and SPP are also commonly observed in the semi-classical Ising spin systems, we should therefore concentrate on QFI, QFO and FRU, in which quantum entanglement of the Heisenberg spin pairs indicates the quantum nature of these phases. It can easily be understood from equations (25) and (28) that QFI and QFO are quite similar one to each other. As a matter of fact, all pairs of Heisenberg spins reside in both phases in the same eigenstate, and thus the only difference between them consists in the spin arrangement of their Ising counterparts. In QFO, which is stable at stronger fields, the Ising spins tend to align towards the external field, whilst they are oriented opposite to the external field in QFI, which is stable at relatively weaker fields. Notice that the quantum entanglement between the pairs of Heisenberg spins that occurs in QFI and QFO can also be understood within the valence-bond-solid picture [65, 66]. If spin-1 sites are decomposed into two spin-$\frac{1}{2}$ variables, then one of the decomposed spins at each spin-1 site forms the singlet dimer with its nearest-neighbouring spin-1 site, while the other one is polarized by the external field. As a result of this incomplete pairing, each spin-1 site effectively acts in QFI and QFO as would the spin-$\frac{1}{2}$ variable. Further, it should be also remarked that all Ising spins are completely free to flip (frustrated) in FRU on behalf of a preferred antiferromagnetic alignment between each pair of Heisenberg spins. Owing to this fact, FRU can be viewed as a state characterized by a complete randomization of the Ising spins, which consequently leads to a macroscopic degeneracy of FRU resembling in its residual entropy $S_{\mathrm{res}}/3N = \ln(2)^{1/3}$.

To clarify the magnetization scenario available for the mixed spin-$\frac{1}{2}$ and spin-1 diamond chain, we depict in figure 8 all possible types of magnetization curves. In agreement with the phase diagram shown in figure 7(b), there are in total four different types of magnetization curves reflecting the transitions FRI–SPP (a), QFI–FRI–SPP (b), FRU–FRI–SPP (c) and FRU–QFO–SPP (d). It should be stressed, nevertheless, that the system undergoes true transitions between these phases merely at zero temperature, where indeed stepwise magnetization curves emerge with abrupt change(s) of the magnetization at critical field(s). However, it is worthy of notice that there are no real magnetization jumps at any finite temperature and the sharp stepwise magnetization curves to be observed at zero temperature are gradually smeared out as temperature increases. It can be clearly seen from figure 8 that an increase in temperature also actually shrinks the width of plateaux until the plateau states completely disappear from the magnetization curves above a certain temperature. The most notable magnetization curves are those with the zero-field ground state corresponding to FRU as shown in figures 8(c) and (d). According to these plots, it can easily be realized that all frustrated Ising spins tend to align to the external-field direction for any finite but non-zero external field provided that temperature is set to zero. At non-zero temperatures, in contrast, the magnetization rises much more steadily in the vicinity of zero field in comparison with the magnetization curves having the long-range-ordered FRI (figure 8(a)) and QFI (figure 8(b)) phases in the ground state. Finally, it is also worthwhile to remark that the observed magnetization plateaux at $\frac{1}{5}$ (QFI and FRU) and $\frac{3}{5}$ (QFO) of the saturation magnetization satisfy the Oshikawa–Yamanaka–Affleck rule [67].

Now, let us investigate in particular an influence of the spin frustration on thermal variations of the zero-field susceptibility times temperature (χt) data. The temperature dependence of the χt product is displayed in figure 9(a) for several values of the frustration parameter α that determine the ground state to be either of FRI or QFI type. Interestingly, χt data then exhibit a round minimum upon cooling, which is followed by an exponentially steep

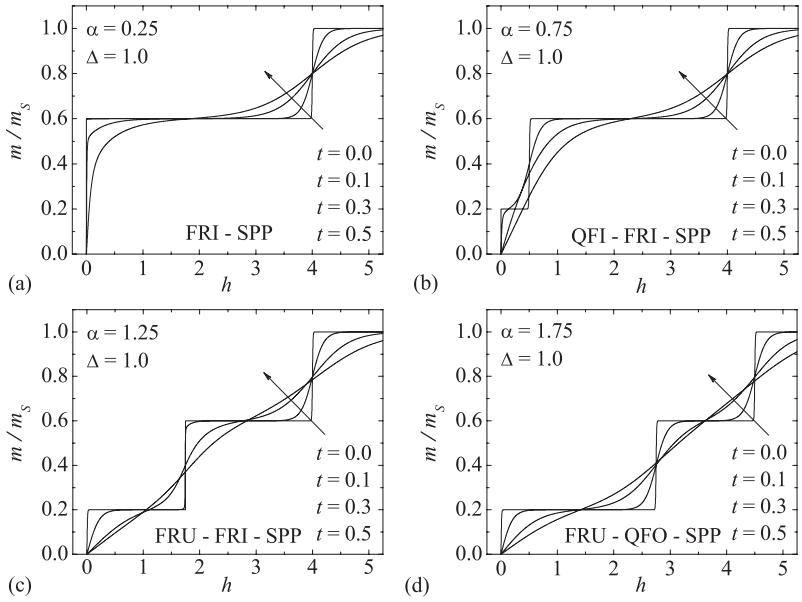

Figure 8. The total magnetization reduced with respect to its saturation value as a function of the external field at various temperatures $t = 0.0, 0.1, 0.3, 0.5$ in ascending order along the direction of arrows.

increase that appears by approaching zero temperature. It is quite obvious from figure 9(a) that the stronger the parameter of frustration α, the deeper the notable minimum whose position is simultaneously shifted towards lower temperatures. It is worth remembering, moreover, that the minimum in the t–χt plot is a typical feature of quantum ferrimagnets [68], and also in our case the minimum becomes especially marked by selecting $\alpha \in (\frac{1}{2}, 1)$ when QFI constitutes the ground state. On the other hand, the temperature dependence of χt data is depicted in figure 9(b) for the case when the frustration parameter $\alpha > 1$ drives the system into the disordered FRU ground state. Under these circumstances, the susceptibility diverges as t^{-1} at low temperatures and the χt product tends to constant value $1/12$ near zero temperature. This value can be interpreted in terms of the Curie law of the frustrated Ising spins, since the spin arrangement that appears in FRU can be viewed as being composed of an independent set of the antiferromagnetic Heisenberg dimers and isolated Ising monomers, whereas the former ones do not contribute to the χt product in the zero-temperature limit.

To gain an insight into overall thermodynamics, let us turn our attention to a thermal behaviour of the specific heat. For this purpose, the zero-field specific heat is plotted against temperature in figures 10(a) and (b) for several values of the frustration parameter α. It can be clearly seen from figure 10(a) that a rounded Schottky-type maximum observable at smaller values of α (e.g. $\alpha = 0.25$) gradually changes, as the frustration strengthens, to a striking dependence with the shoulder superimposed on this round maximum ($\alpha = 0.4$). It is noteworthy that the shoulder becomes more pronounced the closer α is selected to $\alpha_{b1} = 0.5$, determining the phase boundary between FRI and QFI. Under further increase of the frustration the shoulder merges with the Schottky-type maximum, which eventually gives rise to a peculiar non-rounded maximum with almost constant value of the specific heat over a wide temperature range ($\alpha = 0.6$). Next, figure 10(b) shows how the specific heat recovers its double-peak structure when α approaches another phase boundary between QFI and FRU to appear at

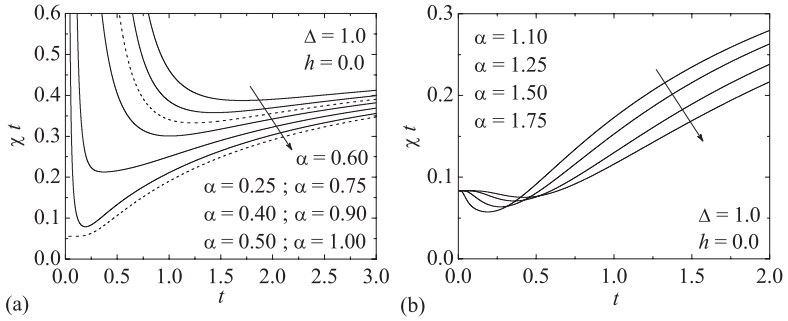

Figure 9. Thermal dependence of the zero-field susceptibility times temperature data for $\Delta = 1.0$, $\alpha = 0.25, 0.4, 0.5, 0.6, 0.75, 0.9, 1.0$ (a) and $\Delta = 1.0$, $\alpha = 1.1, 1.25, 1.5, 1.75$ (b) in ascending order along the direction of arrows. For clarity, the cases $\alpha_{c1} = 0.5$ and $\alpha_{c2} = 1.0$ corresponding to the phase boundaries between FRI–QFI and QFI–FRU, respectively, are depicted as broken lines.

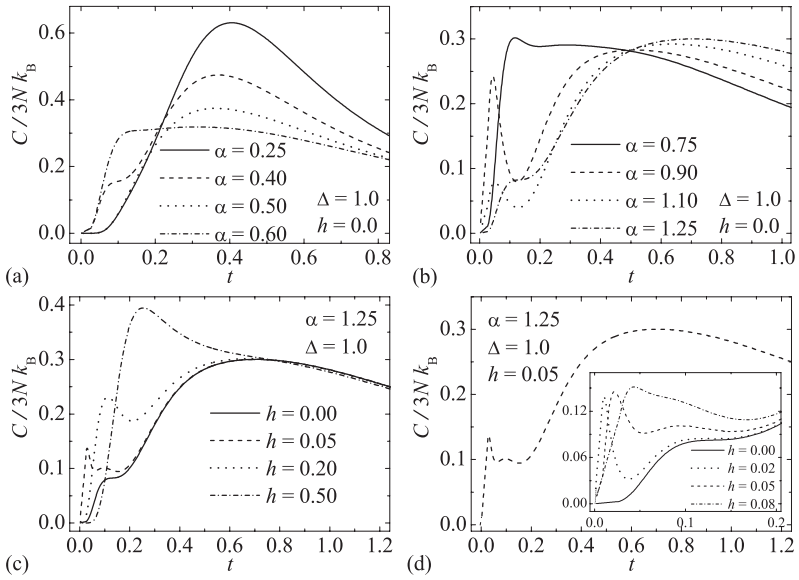

Figure 10. Temperature variations of the specific heat when $\Delta = 1.0$ is fixed. ((a), (b)) illustrate the effect of frustration parameter α on the shape of zero-field specific heat, whereas ((c), (d)) display the effect of applied external field when the frustration parameter $\alpha = 1.25$ drives the system into the disordered FRU state.

$\alpha_{b2} = 1.0$ (see for instance the curves for $\alpha = 0.75$ and 0.9). In addition, it is quite evident from figure 10(b) that repeated strengthening of the frustration results in a suppression of the low-temperature peak until it finally merges with the high-temperature one. Note furthermore that the high-temperature peak has a general tendency to enhance in magnitude (both in height as well as in width) as α increases and its position is shifted towards higher temperatures. Altogether, it might be concluded that the remarkable double-peak structure of the specific heat arises just when the frustration parameter is close enough to a phase boundary. This result is taken to mean that the observed double-peak specific heat curves always originate from thermal excitations to a spin configuration rather close in energy to the ground state.

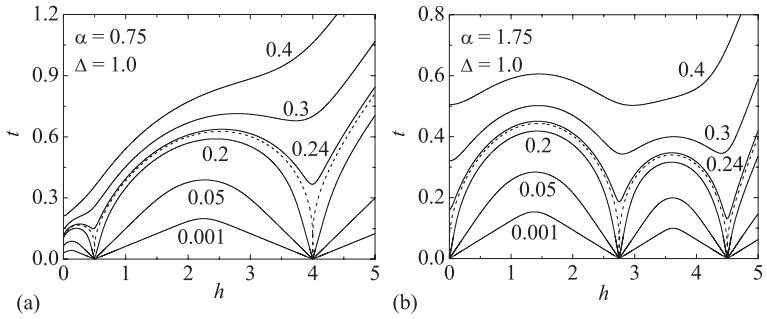

Figure 11. Adiabatic demagnetization in the form of temperature versus external field dependence when $\Delta = 1.0$, $\alpha = 0.75$ (a) and $\Delta = 1.0$, $\alpha = 1.75$ (b). For clarity, the broken curve depicts the dependence when entropy is fixed at the residual value $S_{\rm res}/3N = \ln(2)^{1/3}$ of FRU.

An even more striking situation emerges by turning on the external field. The overall trend of the external field is to increase the height and width of the low-temperature peak and to shift it towards higher temperatures until it coalesces with the higher-temperature maximum. It should be remarked, nevertheless, that the most notable dependences of the specific heat arise from when the frustration leads to the disordered FRU ground state. Besides the afore-described general trends illustrated in figure 10(c), there also appears a remarkable kind of specific heat curve with the triple-peak structure as particularly drawn in figure 10(d) and its inset. Apparently, the additional third peak observable at very low temperatures occurs on applying the small but non-zero external field. It is therefore quite reasonable to conjecture that an origin of this low-temperature peak lies in the field-induced splitting of energy levels related to the frustration of the Ising spins. Actually, the stronger the external field, the greater the splitting caused by the external field and, consequently, the position of this peak steadily shifts towards higher temperatures. Above a certain external field, the additional third peak vanishes because of merging with the low-temperature peak also observable in the zero-field case.

Finally, we shall close our discussion with an exploration of the adiabatic demagnetization examined in connection with the enhanced magnetocaloric effect. Adiabatic processes keeping the entropy constant are plotted in figure 11 in the form of the temperature versus external field dependence. Two displayed sets of demagnetization curves evidently reflect adiabatic change of temperature, which accompanies the transitions SPP $\rightarrow$ FRI $\rightarrow$ QFI (figure 11(a)) and SPP $\rightarrow$ QFO $\rightarrow$ FRU (figure 11(b)). When comparing these results with the ones formerly discussed for the spin-$\frac{1}{2}$ diamond chain (figure 6), one easily finds some similarities between the two investigated diamond chains. Indeed, the most obvious drop in temperature is retrieved once again in the vicinity of critical fields and zero field, where zero temperature is in principle reached whenever the entropy is set equal to or less than its residual value $S_{\rm res}$. Moreover, the enhanced magnetocaloric effect with the cooling rate exceeding the one of paramagnetic salts occurs just as the disordered FRU phase constitutes the ground state and the external field is below $h \approx 0.05$. By contrast, the most obvious difference between the two investigated spin systems consists in the greater diversity of the adiabatic process of the latter (mixed-spin) system, which exhibits dependences with two critical fields in addition to the ones with one critical field only.

4. Conclusion

Exactly solvable frustrated spin systems are currently much sought after in the field of condensed matter physics, since they can serve as useful model systems for in-depth

understanding of the effect of geometric frustration still not fully elucidated yet. In the present work, we have provided rigorous results for one notable example of such a system, the mixed spin-$\frac{1}{2}$ and spin-S Ising–Heisenberg diamond chain tractable within the generalized decoration–iteration map. It is worthy of mention that this rather simple model system has primarily been developed to predict and to understand the behaviour of insulating magnetic materials, in which the Heisenberg dimers interact with the Ising monomers in such a way that they form the diamond chain. Notice that the coordination polymers consisting of the pairs of interacting transition-metal elements (Heisenberg dimers) coupled to the rare-earth elements (Ising monomers) represent perspective experimental realizations of the proposed system. Although we are not aware of any real coordination compound which would meet this requirement, the recent progress in the design and controlled synthesis of the molecular-based magnetic materials supports our hope that it would be possible to prepare such polymeric chains in the near future.

It is worthwhile to remark that a special emphasis is laid in our study on the investigation of geometric frustration generated by the competition between Heisenberg- and Ising-type interactions. Our results clearly demonstrate that an interplay between the frustration and quantum fluctuations, both arising from the Heisenberg exchange interaction, is at the origin of interesting behaviour not commonly observed in the semi-classical Ising spin systems. Indeed, this interplay gives rise to several peculiar ground states with entangled states of Heisenberg spins and quantum effects turned out to play a substantial role in determining their finite-temperature properties as well. Among other matters, we have found rigorous evidence for appearance of the quantized plateaux in the magnetization curves, the round minimum in the temperature dependence of the susceptibility times temperature data, the double-peak zero-field specific heat curves, the enhanced magnetocaloric effect and so on. In our opinion, the most interesting finding to emerge from our study is direct evidence of the triple-peak specific heat curve that appears when applying small external field to the system driven by the frustration into the disordered state. To the best of our knowledge, the discovery and possible explanation of the triple-peak structure in the specific heat curve has not been reported for any frustrated system hitherto.

Last but not least, it should be remarked that the relative ease of the generalized mapping method used here implies a possibility of further extensions. Actually, this approach can straightforwardly be extended to account also for higher-spin values of both Ising as well as Heisenberg spins, the single-ion anisotropy effect, the biquadratic exchange interaction, the next-nearest-neighbour interaction, the multispin interactions, etc. It is also noteworthy that the applied procedure is not constrained either by the lattice topology, and thus it can be utilized for investigating the effect of geometric frustration on the planar Ising–Heisenberg lattices composed of the diamond-shaped units [72, 73]. Our next work continues in this direction.

Acknowledgments

The authors express gratitude to scientific grant agencies VEGA and APVV, supporting this work under grants VEGA 1/2009/05 and APVT 20-005204.

Appendix

Before we list explicit expressions for the functions $G(x)$ and $F_i(x)$ ($i = 1$–4), which enter the transformation formulae (3)–(4) and the set of equations (15)–(17), respectively, let us establish the notation $j_{\mathrm{H}} = \beta J_{\mathrm{H}}$, $h_{\mathrm{H}} = \beta H_{\mathrm{H}}$ and $\delta = \sqrt{1 + 8\Delta^2}$.

(a) Expressions for the spin case $S = \frac{1}{2}$:

$$G(x) = 2\exp(-j_{\mathrm{H}}/4)\cosh(x - h_{\mathrm{H}}) + 2\exp(j_{\mathrm{H}}/4)\cosh(j_{\mathrm{H}}\Delta/2),$$
$$F_1(x) = -\exp(-j_{\mathrm{H}}/4)\sinh(x - h_{\mathrm{H}})/G(x),$$
$$F_2(x) = [\exp(j_{\mathrm{H}}/4)\cosh(j_{\mathrm{H}}\Delta/2) - \exp(-j_{\mathrm{H}}/4)\cosh(x - h_{\mathrm{H}})]/\big[2G(x)\big],$$
$$F_3(x) = -\exp(j_{\mathrm{H}}/4)\sinh(j_{\mathrm{H}}\Delta/2)/\big[2G(x)\big],$$
$$F_4(x) = 1/4.$$

(b) Expressions for the spin case $S = 1$:

$$G(x) = 2\exp(j_{\mathrm{H}}/2)\cosh(j_{\mathrm{H}}\delta/2) + 2\exp(-j_{\mathrm{H}})\cosh[2(x - h_{\mathrm{H}})] + \exp(j_{\mathrm{H}}) + 4\cosh(x - h_{\mathrm{H}})\cosh(j_{\mathrm{H}}\Delta),$$
$$F_1(x) = -\{2\exp(-j_{\mathrm{H}})\sinh[2(x - h_{\mathrm{H}})] + 2\sinh(x - h_{\mathrm{H}})\cosh(j_{\mathrm{H}}\Delta)\}/G(x),$$
$$F_2(x) = \{2\exp(-j_{\mathrm{H}})\cosh[2(x - h_{\mathrm{H}})] - \exp(j_{\mathrm{H}}) - \delta\mathcal{C} - \mathcal{S}\}/G(x),$$
$$F_3(x) = -\{2\cosh(x - h_{\mathrm{H}})\sinh(j_{\mathrm{H}}\Delta) + 4\Delta\mathcal{S}\}/G(x),$$
$$F_4(x) = \{2\exp(-j_{\mathrm{H}})\cosh[2(x - h_{\mathrm{H}})] + \exp(j_{\mathrm{H}}) + 2\cosh(x - h_{\mathrm{H}})\cosh(j_{\mathrm{H}}\Delta) + \delta\mathcal{C} + \mathcal{S}\}/G(x),$$

where $\mathcal{S} = \exp(j_{\mathrm{H}}/2)\sinh(j_{\mathrm{H}}\delta/2)/\delta$ and $\mathcal{C} = \exp(j_{\mathrm{H}}/2)\cosh(j_{\mathrm{H}}\delta/2)/\delta$.

References

[1] Toulouse G 1977 *Commun. Phys.* **2** 115
[2] Greedan J E 2001 *J. Mater. Chem.* **11** 37–53
[3] Diep H T (ed) 2004 *Magnetic Systems with Competing Interaction* (Singapore: World Scientific)
[4] Villain J, Bidaux R, Carton J P and Conte R J 1980 *J. Physique* **41** 1263
[5] Villain J 1977 *J. Phys. C: Solid State Phys.* **10** 1717–34
[6] Sachdev S 1999 *Quantum Phase Transitions* (Cambridge: Cambridge University Press)
[7] Richter J, Krüger S, Farnell D and Bishop R 2001 *Quantum Phase Transitions in Spin Systems* (*Series on Advances in Quantum Many-Body Theory* vol 3) ed R F Bishop, K A Gernoth and N R Walet (Singapore: World Scientific) pp 239–46
[8] Richter J, Schulenburg J and Honecker A 2004 *Quantum Magnetism* (*Springer Lecture Notes in Physics* vol 645) ed U Schollwöck, J Richter, D Farnell and R Bishop (Berlin: Springer) pp 85–129
[9] Miyahara S and Ueda K 2003 *J. Phys.: Condens. Matter* **15** R327–R366
[10] Honecker A, Schulenburg J and Richter J 2004 *J. Phys.: Condens. Matter* **16** S749–58
[11] Kubo K 1993 *Phys. Rev.* B **48** 10552–5
[12] Nakamura T and Kubo K 1996 *Phys. Rev.* B **53** 6393–400
[13] Maisinger K and Schollwöck U 1998 *Phys. Rev. Lett.* **81** 445–8
[14] Zhitomirsky M E 2003 *Phys. Rev.* B **67** 104421
[15] Zhitomirsky M E and Honecker A 2004 *J. Stat. Mech.* P07012
[16] Honecker A and Richter J 2005 *Condens. Matter Phys.* **8** 813–24
[17] Derzhko O and Richter J 2006 *Preprint* cond-mat/0604023
[18] Majumdar C K and Ghosh D K 1969 *J. Math. Phys.* **10** 1388–98
[19] Majumdar C K and Ghosh D K 1969 *J. Math. Phys.* **10** 1399–402
[20] Majumdar C K 1970 *J. Phys. C: Solid State Phys.* **3** 911–5
[21] van den Broek P M 1980 *Phys. Lett.* A **77** 261–2
[22] Doucot B and Kanter I 1989 *Phys. Rev.* B **39** 12399–402
[23] Monti F and Sütö A 1991 *Phys. Lett.* A **156** 197–200
[24] Monti F and Sütö A 1992 *Helv. Phys. Acta* **65** 560–95
[25] Sen D, Shastry B S, Walstedt R E and Cava R 1996 *Phys. Rev.* B **53** 6401–5
[26] Shastry B S and Sutherland B 1981 *Physica* B+C **108** 1069–70
[27] Takano K, Kubo K and Sakamoto H 1996 *J. Phys.: Condens. Matter* **8** 6405–11
[28] Okamoto K, Tonegawa T, Takahashi Y and Kaburagi M 1999 *J. Phys.: Condens. Matter* **11** 10485–98
[29] Wang H T 2002 *J. Phys.: Condens. Matter* **14** 8033–42

[30] Tonegawa T, Okamoto K, Hikihara T, Takahashi Y and Kaburagi M 2000 *J. Phys. Soc. Japan* **69** 332–8
[31] Tonegawa T, Okamoto K, Hikihara T, Takahashi Y and Kaburagi M 2001 *J. Phys. Chem. Solids* **62** 125–8
[32] Okamoto K, Tonegawa T and Kaburagi M 2003 *J. Phys.: Condens. Matter* **15** 5979–95
[33] Sano K and Takano K 2000 *J. Phys. Soc. Japan* **69** 2710–1
[34] Honecker A and Läuchli A 2001 *Phys. Rev.* B **63** 174407
[35] Okamoto K and Ichikawa Y 2002 *J. Phys. Chem. Solids* **63** 1575–7
[36] Okamoto K, Tokuno A and Ichikawa Y 2005 *J. Phys. Chem. Solids* **66** 1442–5
[37] Niggemann H, Uimin G and Zittartz J 1997 *J. Phys.: Condens. Matter* **9** 9031–42
[38] Niggemann H, Uimin G and Zittartz J 1998 *J. Phys.: Condens. Matter* **10** 5217–36
[39] Pati S K 2003 *Phys. Rev.* B **67** 184411
[40] Vitoriano C, De Brito F B, Raposo E P and Coutinho-Filho M D 2002 *Mol. Cryst. Liq. Cryst.* **374** 185–90
[41] Vitoriano C, Coutinho-Filho M D and Raposo E P 2002 *J. Phys. A: Math. Gen.* **35** 9049–61
[42] Ramirez A 1994 *Annu. Rev. Mater. Sci.* **24** 453–80
[43] Zigan F and Schuster H D 1972 *Z. Kristallogr.* **135** 416
[44] Kikuchi H, Fujii Y, Chiba M, Mitsudo S and Idehara T 2003 *Physica* B **329–333** 967–8
[45] Kikuchi H, Fujii Y, Chiba M, Mitsudo S, Idehara T and Kuwai T 2004 *J. Magn. Magn. Mater.* **272–276** 900–1
[46] Kikuchi H, Fujii Y, Chiba M, Mitsudo S, Idehara T, Tonegawa T, Okamoto K, Sakai T, Kuwai T and Ohta H 2004 *Phys. Rev. Lett.* **94** 227201
[47] Kikuchi H, Fujii Y, Chiba M, Mitsudo S, Idehara T, Tonegawa T, Okamoto K, Sakai T, Kuwai T, Kindo K, Matsuo A, Higemoto W, Nishiyama K, Horvatic M and Bertheir C 2005 *Prog. Theor. Phys.* **159** 1–10
[48] Ohta H, Okubo S, Kamikawa T, Kunimoto T, Inagaki Y, Kikuchi H, Saito T, Azuma M and Takano M 2003 *J. Phys. Soc. Japan* **72** 2464–7
[49] Okubo S, Kamikawa T, Kunimoto T, Inagaki Y, Ohta H, Nojiri H and Kikuchi H 2004 *J. Magn. Magn. Mater.* **272–276** 912–3
[50] Ohta H, Okubo S, Inagaki Y, Hiroi Y and Kikuchi H 2004 *Physica* B **346/347** 38–44
[51] Okubo S, Ohta H, Inagaki Y and Sakurai T 2004 *Physica* B **346/347** 627–32
[52] Okubo S, Taketani A, Ohta H, Kunimoto T, Inagaki Y, Saito T, Azuma M, Takano M and Kikuchi H 2005 *Prog. Theor. Phys.* **159** 11–6
[53] Belaiche M, Drillon M, Aride J, Boukhari A, Biaz T and Legoll P 1991 *J. Chim. Phys.* PCB **88** 1713–9
[54] Guillou N, Pastre S, Livage C and Ferey G 2002 *Chem. Commun.* 2358–9
[55] Konar S, Mukherjee P S, Zangrado E, Lloret F and Chaudhuri N R 2002 *Angew. Chem. Int. Edn* **41** 1561–3
[56] Humphrey S M and Wood P T 2004 *J. Am. Chem. Soc.* **126** 13236–7
[57] Tong M L, Wang J and Hu S 2005 *J. Solid State Chem.* **178** 1518–25
[58] Fisher M E 1959 *Phys. Rev.* **113** 969–81
[59] Syozi I 1972 *Phase Transitions and Critical Phenomena* vol 1, ed C Domb and M S Green (New York: Academic) pp 269–329
[60] Strečka J and Jaščur M 2002 *Czech. J. Phys.* **52** A39–A42
[61] Strečka J and Jaščur M 2003 *J. Phys.: Condens. Matter* **15** 4519–34
[62] Strečka J, Jaščur M, Hagiwara M and Minami K 2004 *Czech. J. Phys.* **54** D583–6
[63] Strečka J, Jaščur M, Hagiwara M, Minami K, Narumi Y and Kindo K 2005 *Phys. Rev.* B **72** 024459
[64] Lavis D A and Bell G M 1999 *Statistical Mechanics of Lattice Systems* vol 1 (Berlin: Springer)
[65] Affleck I, Kennedy T, Lieb E H and Tasaki H 1987 *Phys. Rev. Lett.* **59** 799–802
[66] Affleck I, Kennedy T, Lieb E H and Tasaki H 1988 *Commun. Math. Phys.* **115** 477–528
[67] Oshikawa M, Yamanaka M and Affleck I 1997 *Phys. Rev. Lett.* **78** 1984–7
[68] Yamamoto S, Fukui T, Maisinger K and Schollwöck U 1998 *J. Phys.: Condens. Matter* **10** 11033–48
[69] Yamamoto S 1999 *Phys. Rev.* B **59** 1024–7
[70] Nakanishi T and Yamamoto S 2002 *Phys. Rev.* B **65** 214418
[71] Yamamoto S 2004 *Phys. Rev.* B **69** 064426
[72] Strečka J and Jaščur M 2002 *Phys. Status Solidi* b **233** R12–4
[73] Strečka J and Jaščur M 2006 *Acta Phys. Slovaca* **56** 65–70